

Heuristic approach to trajectory correlation functions in bounded regions with Lambert scattering walls

T. Rao and R. Golub

Physics Department, North Carolina State University, Raleigh, North Carolina 27695, USA

The behavior of spins undergoing Larmor precession in the presence of time varying fields is of interest to many research fields. The frequency shifts and relaxation resulting from these fields are related to their power spectrum and can be determined from the Fourier Transform of the auto-correlation functions of the time varying field. Using the method of images [C. M. Swank, A. K. Petukhov, and R. Golub, *Phys. Lett. A* **376**, 2319 (2012)] calculated the position-position auto-correlation function for particles moving in a rectangular cell with specular scattering walls. In this work we present a heuristic model that extends this work to the case of Lambert scattering walls. The results of this model are compared to simulation and show good agreement from the ballistic to diffusive regime of gas collisions, for both square and general rectangular cells. This model requires three parameters, two of which describe the distribution of images in the case of a square cell, and one of which describes the asymmetry in the mixing of the x and y components of the velocity in the case of non-square rectangular cells.

INTRODUCTION

Systems of spins moving under the influence of static and time varying magnetic fields are of wide-ranging scientific interest. It was Bloembergen, Purcell, and Pound [1] who first showed that the relaxation time of the spins is given by the power spectrum of the fluctuating field evaluated at the Larmor frequency. In general, the power spectra can be written in terms of the Fourier transform of the auto-correlation function of the fluctuating field. See the introductions of [2, 3] for a brief history of the field.

One of the applications of these techniques is in next generation neutron electric dipole moment (nEDM) searches, which require measurements of spin dynamics at the nanohertz level. Additionally the motional magnetic field resulting from the interaction between the spins and the electric field in such experiments results in “false EDM” systematic error that needs to be accounted for [4]. Redfield [5], Slichter [6], and McGregor [7] have given formal derivations of the relation between relaxation and the auto-correlation functions of the fields, and the method was applied to the “false EDM” [4] systematic error in nEDM searches [8]. General methods for calculating auto-correlation functions for particles diffusing in inhomogeneous fields can be found in [9, 10].

Additionally, methods for calculating the trajectory auto-correlation functions, or the frequency shift resulting from the motional magnetic field have been developed for a variety of geometries, wall conditions, and collision rates. Barabanov et al [11] used a calculation of the velocity-velocity correlation function for individual ballistic trajectories to obtain the motional field frequency shift in the case of a circular cell with specular scattering walls. This result was expanded to include the effect of gas collisions by noting the spectrum was a sum of harmonic oscillators, and including a damping term to model the gas collisions. The work of Golub, Steyerl et al [12, 13] similarly considered cylindrical cells

in terms of individual ballistic trajectories, but now with diffuse Lambert scattering walls. Additionally, the case of square and more general rectangular cells for specular and Lambert scattering walls were solved for. However, noticeable qualitative differences between their calculation and simulation exist in the case of non-square rectangular cells with Lambert scattering walls. Specifically, simulation shows two peaks in the spectrum, while their calculation only shows one. Clayton [14] also considers the case of rectangular cells, but in the diffusive limit rather than the ballistic limit, and uses the conditional probability of finding the particle at a position inside the cell to calculate the trajectory correlation functions. This work covers the 1D, 2D, and 3D cells but only works when gas collisions are frequent enough that the diffusion equation is valid. This work was expanded upon by Swank et al [15, 16] giving solutions for 1D, 2D, and 3D rectangular cells that apply from the ballistic to diffusive limit, but only in the case of specular wall collisions.

The method in [15, 16] utilizes the method of images by applying the conditional probability of finding a particle at position r , given initial position r_0 , and travel time τ , for an unbounded domain [17]. As explained in Fig. 1 going from the real cell to the image cells can be represented by a triangle wave periodic extension $\vec{r}_0(r_0)$.

In this work we extend the technique of Swank et al to non specular wall conditions, specifically the case of Lambert scattering walls. We alter the position of the images in an attempt to alter the scattering angle at the wall. This is accomplished by introducing a distribution of reflecting wall positions. The properties of the image distribution required to reproduce Lambert scattering is determined by comparing the resulting spectrum of the trajectory correlation function to simulation. In this way we develop an heuristic model of 2D rectangular cells with Lambert scattering walls that’s valid from the ballistic to diffusive regime. Previously, Lambert scattering walls have only been considered in the ballistic limit [12],

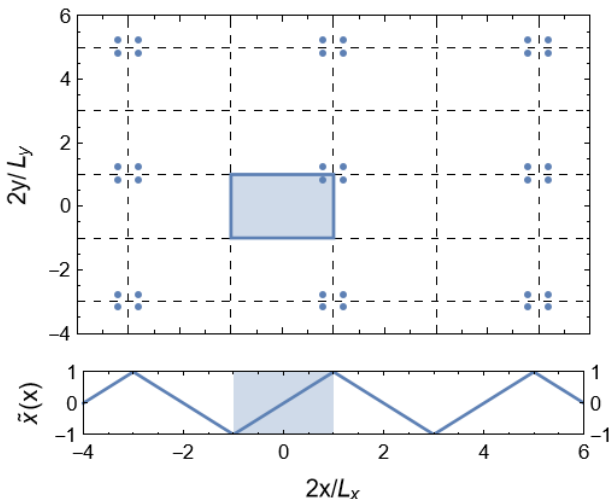


FIG. 1. The physical region (shaded) and a few of the periodic image cells for the case of specular scattering walls described in [15]. The shown image positions all correspond to the same source inside the physical cell. Trajectories between an image and an observation point correspond to a trajectory between the source point and the observation point that has undergone the same number of wall collisions as image cell walls intersected by the image trajectory. The walls of the physical cell are located at $x = \pm L_x/2$ and $y = \pm L_y/2$. The field in the physical region, in this case $B(x) = x$, is mirrored at the boundary between image cells so that images see the same field as the source. This results in a periodic extension of the position inside the cell $\tilde{x}(x)$, in this case a triangle wave, over the infinite domain.

giving results that agree with simulation in the case of cylindrical and square cells, but not in the case of rectangular cells.

THE POSITION-POSITION TRAJECTORY CORRELATION FUNCTION FOR LAMBERT SCATTERING WALLS

From [15] Eq. (10) we see we can write the position-position trajectory correlation function as

$$\langle \vec{r}_0(t) \cdot \vec{r}(t + \tau) \rangle = \frac{1}{L_x L_y} \int \int d^2 r_0 d^2 r \vec{r}_0(r_0) \cdot \vec{r} P(\vec{r} - \vec{r}_0, \tau) \quad (1)$$

with the infinite domain conditional probability $P(\vec{r} - \vec{r}_0, \tau)$ from [17]. The method of images allows the use of the infinite domain conditional probability. The conditional probability of a trajectory in a finite domain is replaced by the infinite domain conditional probability between the image position r_0 , and the observation point inside the physical cell r , for travel time τ . The dot product is evaluated using the periodic extension of the physical cell $\vec{r}_0(r_0)$ for the source position.

From Eq. (1) the 1D correlation function from [15, 16] for a 2D cell can be written as

$$\langle \tilde{x}_0(t)x(t + \tau) \rangle = \frac{1}{L_x} \int_{-\infty}^{\infty} \int_{-L_x/2}^{L_x/2} dx_0 dx \tilde{x}_0(x_0)xP(\vec{r} - \vec{r}_0, \tau) \quad (2)$$

To get the Spectrum we must take the Fourier transform of Eq. (1). From [17] we know the Fourier-Laplace transform of the 2D infinite domain conditional probability is given by

$$P(\vec{q}, s) = \frac{t_c}{\sqrt{(t_c v q)^2 + (1 + s t_c)^2 - 1}} \quad (3)$$

where t_c is the mean gas collisions time, and v is the particle speed. If we use an even extension of the conditional probability to negative τ the Fourier transform of $P(\vec{r} - \vec{r}_0, \tau)$ is a real even function equal to $2\text{Re}[\int_0^{\infty} P(r, t)e^{-i\omega t} dt]$. This is simply twice the real part of the Laplace transform of $P(r, t)$ for $s = i\omega$ giving us

$$S_{xx}(\omega) = \frac{2}{L_x} \text{Re} \left[\int_{-\infty}^{\infty} \int_{-L_x/2}^{L_x/2} dx_0 dx \tilde{x}_0(x_0)xP(\vec{r} - \vec{r}_0, i\omega) \right] \quad (4)$$

where $S_{xx}(\omega)$ is the spectrum of 1D correlation function, and $P(\vec{r} - \vec{r}_0, s = i\omega)$ is the Laplace transform of $P(\vec{r} - \vec{r}_0, \tau)$. Additionally we can rewrite $P(\vec{r} - \vec{r}_0, i\omega)$ as $\int d\vec{q} P(\vec{q}, i\omega) \frac{e^{i\vec{q} \cdot (\vec{r} - \vec{r}_0)}}{2\pi}$, where $P(\vec{q}, i\omega)$ is the Fourier-Laplace transform given in Eq. (3). Since the conditional probability for an infinite domain has no angular dependence we can choose $\vec{q} = q\hat{x}$ without loss of generality. This in turn results in

$$S_{xx}(\omega) = \frac{2}{2\pi L_x}$$

$$\times \text{Re} \left[\int_{-\infty}^{\infty} dq \int_{-L_x/2}^{L_x/2} dx \int_{-\infty}^{\infty} dx_0 P(q, i\omega) e^{iq(x-x_0)} \tilde{x}_0 x \right] \quad (5)$$

or equivalently

$$S_{xx}(\omega) = \frac{2}{2\pi L_x}$$

$$\times \text{Re} \left[\int_{-\infty}^{\infty} dq P(q, i\omega) \int_{-L_x/2}^{L_x/2} dx e^{iqx} x \int_{-\infty}^{\infty} dx_0 e^{iqx_0} \tilde{x}_0 \right] \quad (6)$$

For specular walls, a trajectory's wall reflection is accounted for by a single image position, since the reflected angle is exactly determined by the incoming angle. For rough walls the reflected angle is random and follows a cosine distribution. Because of this a single image is no longer sufficient to describe the scattering. Instead there exists a distribution of image positions that correspond to the possible reflected trajectories (different observation points), or equivalently, each image position can be thought of as corresponding to multiple possible sources inside the physical cell. If the specular image is altered by changing the size of the image cells, the \tilde{x}_0 corresponding to a given image is also altered. We attempt to find a distribution of image cell sizes that generate the correct distribution of \tilde{x}_0 to reproduce Lambert wall scattering when calculating the trajectory correlation function. The distribution of image cell sizes that corresponds to Lambert scattering can then be used to calculate an effective extension to the x axis that can be used in place of the specular periodic extension.

In [15, 16] the image positions for specular walls are accounted for by a triangle wave extension of the particle's position outside of the cell (See Fig. 1)

$$\tilde{x}_0(x_0) = \sum_{n=\text{odd}} \frac{-i^{n2} L_x}{\pi^2 n^2} e^{i \frac{\pi n}{L_x} x_0} \quad (7)$$

So for Lambert scattering walls we need an appropriate ensemble average of triangle wave extensions that will reproduce the wall scattering. This amounts to taking an ensemble average of triangle waves with different periods l , which would correspond to the length of a side of the physical cell in the case of specular scattering (Eq. (8)). Additionally we average the x and y dimensions separately since we want to include all combinations of l_y and l_x . Note that for a square cell the symmetry in the real cell suggests the distribution of l_x and l_y should be the same. Consequently, in the case of a square cell, although the individual image cells being averaged over are rectangles, l_x and l_y are statistically independent, the effective cell will still be a square.

$$\tilde{x}_0(x_0) = \sum_{\text{odd}} \left\langle \frac{-i^{n2} l}{\pi^2 n^2} e^{i \frac{\pi n}{l} x_0} \right\rangle \quad (8)$$

If we assume a Gaussian distribution in l with average value $L_{\text{mod}x}$, and with width σ , Eq. (8) becomes

$$\tilde{x}_0(x_0) = \sum_{\text{odd}} \frac{-i^{n2}}{\pi^2 n^2} \int_0^{\infty} l e^{i \frac{\pi n}{l} x_0} \frac{e^{-\frac{(l-L_{\text{mod}x})^2}{2\sigma^2}}}{\sqrt{2\pi}\sigma} dl \quad (9)$$

Two examples comparing the x axis extension for Lambert scattering walls given by Eq. (9) to the specular extension given by Eq. (7) are plotted in Fig. 2.

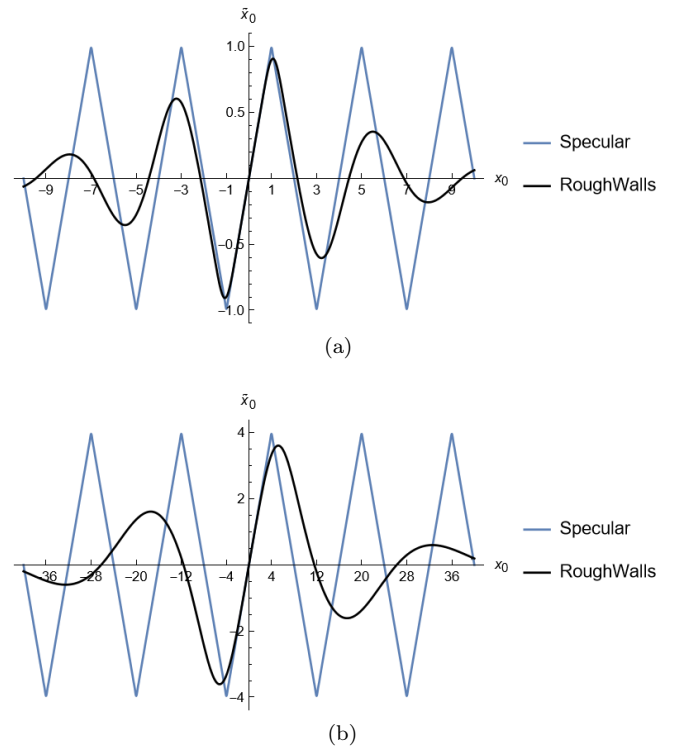


FIG. 2. Specular and rough wall extensions used to account for wall scattering for a square and rectangular cell. (a) The specular and rough wall extensions for a square cell with $L_x = 2$, $L_{\text{mod}x} = 2.13$, and $\sigma = 0.393$. Note the region between -1 and 1 corresponding to the physical cell is barely altered from the specular result. (b) The specular and rough wall extensions for the long side of a rectangular cell with an aspect ratio of 4, $L_{\text{mod}x} = 10.08$, and $\sigma = 3.93$. The length of the sides are normalized to 1/2 of the length of the shorter side. Note the region between -4 and 4 corresponding to the physical cell begins to significantly deviate from the specular case near the walls of the physical cell.

In order to calculate the spectrum of the correlation function, Eq. (6), we need to take the Fourier transform of Eq. (9) giving

$$\tilde{x}_0(q) = \sum_{\text{odd}} \frac{-i^{n2}}{\pi^2 n^2} \int_{-\infty}^{\infty} \int_0^{\infty} l \frac{e^{-\frac{(l-L_{\text{mod}x})^2}{2\sigma^2}}}{\sqrt{2\pi}\sigma} e^{i \frac{\pi n}{l} x_0} e^{-iqx_0} dx_0 dl \quad (10)$$

evaluating the x_0 integral gives us

$$\tilde{x}_0(q) = \sum_{\text{odd}} \frac{-i^{n2}}{\pi^2 n^2} \int_0^{\infty} l \frac{e^{-\frac{(l-L_{\text{mod}x})^2}{2\sigma^2}}}{\sqrt{2\pi}\sigma} 2\pi \delta\left(\frac{n\pi}{l} - q\right) dl \quad (11)$$

we then use the substitution $u = \frac{n\pi}{l}$ and evaluate the delta function

$$\begin{aligned}\tilde{x}_0(q) &= \sum_{\text{odd}} -i^n \frac{2\sqrt{2\pi}}{\sigma} \int_0^\infty e^{-\frac{(\frac{n\pi}{u} - L_{\text{mod}x})^2}{2\sigma^2}} \delta(u - q) \frac{1}{u^3} du \\ &= \sum_{\text{odd}} -i^n \frac{2\sqrt{2\pi}}{\sigma |q|^3} e^{-\frac{(\frac{n\pi}{q} - L_{\text{mod}x})^2}{2\sigma^2}}\end{aligned}\quad (12)$$

The magnitude of q used in the denominator of Eq. (12) is needed to account for the case of negative n and consequently negative q . We now define $q_{x0} = n\pi/L_{\text{mod}x}$ and rewrite this as

$$\tilde{x}_0(q) = \sum_{\text{odd}} -i^n \frac{4\pi}{L_{\text{mod}x} q^2} \frac{n\pi}{\sqrt{2\pi}} \frac{e^{-\frac{n^2 \pi^2 (q_{x0} - q)^2}{2(\sigma^2 q^2 q_{x0}^2)}}}{(|q| \sigma q_{x0})} \quad (13)$$

From Eq. (13) we now have $\int dx e^{-iqx_0} \tilde{x}_0(x_0)$. Additionally we can evaluate the x integral in Eq. (6) to get

$$\int_{-L_x/2}^{L_x/2} dx e^{iqx} x = -\frac{i}{q^2} [qL_x \cos(\frac{qL_x}{2}) - 2 \sin(\frac{qL_x}{2})] \quad (14)$$

and we can now, using Eq. (13) and Eq. (14), write S_{xx} , Eq. (6), as

$$S_{xx} = \frac{4}{L_x L_{\text{mod}x}} \text{Re} \left[\sum_{\text{odd}} i^{n+1} \int_{-\infty}^{\infty} dq P(q, i\omega) \frac{1}{q^4} [qL_x \cos(\frac{qL_x}{2}) - 2 \sin(\frac{qL_x}{2})] \frac{n\pi}{\sqrt{2\pi}} \frac{e^{-\frac{n^2 \pi^2 (q_{x0} - q)^2}{2(\sigma^2 q^2 q_{x0}^2)}}}{(|q| \sigma q_{x0})} \right] \quad (15)$$

For a square $S_{xx} = S_{yy}$ and therefore the 2D spectrum S_{rr} is simply $2S_{xx}$. For a more general rectangle we could write

$$\begin{aligned}S_{rr} &= \frac{4}{L_x L_{\text{mod}x}} \text{Re} \left[\sum_{\text{odd}} i^{n+1} \int_{-\infty}^{\infty} dq P(q, i\omega) \frac{1}{q^4} [qL_x \cos(\frac{qL_x}{2}) - 2 \sin(\frac{qL_x}{2})] \frac{n\pi}{\sqrt{2\pi}} \frac{e^{-\frac{n^2 \pi^2 (q_{x0} - q)^2}{2(\sigma_x^2 q^2 q_{x0}^2)}}}{(|q| \sigma_x q_{x0})} \right] \\ &+ \frac{4}{L_y L_{\text{mod}y}} \text{Re} \left[\sum_{\text{odd}} i^{n+1} \int_{-\infty}^{\infty} dq P(q, i\omega) \frac{1}{q^4} [qL_y \cos(\frac{qL_y}{2}) - 2 \sin(\frac{qL_y}{2})] \frac{n\pi}{\sqrt{2\pi}} \frac{e^{-\frac{n^2 \pi^2 (q_{y0} - q)^2}{2(\sigma_y^2 q^2 q_{y0}^2)}}}{(|q| \sigma_y q_{y0})} \right]\end{aligned}\quad (16)$$

similarly to the case of specular walls [15]. However, unlike specular wall collisions which preserve the magnitude of v_x and v_y individually, Lambert wall collisions mix the x and y components only preserving the overall magnitude of the velocity, in the case of elastic collisions considered here. For a square cell the symmetry between x and y means on average the x and y components aren't effected by the velocity mixing. However, for rectangular cells, $L_y > L_x$ and the velocity mixing is no longer symmetric. Each wall collision results in change in the y velocity relative to the x velocity which needs to be accounted for. Since the solution of a square cell is given by S_{xx} we can account for this effect by altering the velocity used in calculating S_{yy} relative to the nominal velocity in S_{xx} . We note the velocity only appears in the conditional probability and assume a Gaussian in effective speed for calculating S_{yy} giving

$$P(q, i\omega) \rightarrow \int_0^\infty P(v, q, i\omega) \frac{e^{-\frac{(v - v_{nom})^2}{2\sigma_v^2}}}{\sqrt{2\pi}\sigma_v} dv \quad (17)$$

Where the average speed v_{nom} is determined from the ballistic time t_b for a square cell with sides of length L_x . The ballistic time is taken to be the minimum time required to travel from the center of a square cell to one of the walls. This then gives $v_{nom} = \frac{L_x}{2t_b}$. For simplicity we will take $L_x = 2$, and measure times in units of t_b so that $v_{nom} = 1$.

However a Gaussian distribution cannot be exactly correct as the speed cannot be less than zero, and a Gaussian allows for negative values if the standard deviation is large enough. We will show that the width of the Gaussian is ≈ 0.4 in the ballistic limit for a 2x8 cell. Which results in $\approx 0.6\%$ of the Gaussian's area being less than

zero. By changing the integral so the distribution is cut-off for $v < 0.1v_{nom}$ we have now have

$$\int_{0.1}^{\infty} P(v, q, i\omega) \frac{e^{-\frac{(v-1)^2}{2\sigma_v^2}}}{\sqrt{2\pi}\sigma} dv = P_v(q, i\omega, \sigma_v) \quad (18)$$

and problems at small v due to the the unphysical Gaus-

sian tail are removed while only effecting $\approx 1.2\%$ of the area of the probability distribution for a 2×8 cell. Above $v=0.1$ the Gaussian approximation works well.

Applying this change to the conditional probability we then have

$$\begin{aligned} S_{rr} = & \frac{4}{L_x L_{modx}} \text{Re} \left[\sum_{odd} i^{n+1} \int_{-\infty}^{\infty} dq P(q, i\omega) \frac{1}{q^4} [qL_x \cos(\frac{qL_x}{2}) - 2 \sin(\frac{qL_x}{2})] \frac{n\pi}{\sqrt{2\pi}} \frac{e^{-\frac{n^2 \pi^2 (q_{x0} - q)^2}{2(\sigma_x^2 q^2 q_{x0}^2)}}}{(|q| \sigma_x q_{x0})} \right] \\ & + \frac{4}{L_y L_{mody}} \text{Re} \left[\sum_{odd} i^{n+1} \int_{-\infty}^{\infty} dq P_v(q, i\omega, \sigma_v) \frac{1}{q^4} [qL_y \cos(\frac{qL_y}{2}) - 2 \sin(\frac{qL_y}{2})] \frac{n\pi}{\sqrt{2\pi}} \frac{e^{-\frac{n^2 \pi^2 (q_{y0} - q)^2}{2(\sigma_y^2 q^2 q_{y0}^2)}}}{(|q| \sigma_y q_{y0})} \right] \end{aligned} \quad (19)$$

Additionally we can recover the specular limit from Eq. (15) by taking σ_x goes to zero and L_{modx} goes to L_x . Taking this limit $\frac{n\pi}{\sqrt{2\pi}} \frac{e^{-\frac{n^2 \pi^2 (q_0 - q)^2}{2(\sigma^2 q^2 q_0^2)}}}{(|q| \sigma q_0)} \rightarrow \delta(q_{x0} - q)$, giving

$$\begin{aligned} S_{xx} = & -\frac{8}{L_x^2} \sum_{odd} \text{Re} \left[P(q_{x0}, i\omega) \left(\frac{1}{q_{x0}} \right)^4 i^{n+1} \sin(n\pi/2) \right] \\ = & \frac{8}{L_x^2} \sum_{odd} \text{Re} [P(q_{x0}, i\omega)] \left(\frac{1}{q_{x0}} \right)^4, \end{aligned}$$

the expected specular result. In the limit of large gas collision rate ($\lambda = t_b/t_c = 1/t_c$) the wall collisions will be suppressed by the gas collisions, and the Lambert scattering walls and specular walls results should be equal. Therefore σ in this limit should tend toward zero and L_{modx} to L_x . Additionally for rectangular cells in this limit we should see that σ_v goes to zero (as the velocity mixing from wall collisions becomes negligible) so that $P_v \rightarrow P$.

MODEL OF GAS COLLISION RATE DEPENDENCE OF THE PARAMETERS OF THE GAUSSIANS

One way to consider the gas collision rate dependence of the correlation function is that a trajectory that undergoes a gas collision but not a wall collision should be accurately represented by the specular solution, as it doesn't interact with the walls. Therefore as the rate of

gas collisions increase we should expect to see more trajectories like this and the ensemble average of triangle wave extensions from Eq. (8) will move toward a narrower distribution closer to being centered on L . Therefore it's reasonable to think L_{mod} and σ should go like the fraction of wall collisions to total collisions, which can be written as

$$N_w/N = \frac{N_w}{N_w + N_g} = \frac{1}{1 + N_g/N_w} \quad (20)$$

where N_w is the number of wall collisions, N is the total number of collisions, and N_g is the number of gas collisions. In order to understand the gas collisions' contribution let us consider the number of gas collisions per wall collisions in a square cell with sides L . Describing the gas collisions as a 2D random walk the number of gas collisions that occur while traveling a distance d is $N_g = (d/l_{mfp})^2$, where l_{mfp} is the mean free path. Given that $v = 1$, and the gas collision rate $\lambda = 1/t_c$, then $l_{mfp} = vt_c = 1/\lambda$. On average, a wall collision will occur after traveling a distance $L/2$ in 1D. Therefore adjusting for the the 4 walls (and therefore 4 wall collisions) of a square cell, the number of gas collisions per wall collision in the 1D correlation function for a 2D cell (S_{xx} or S_{yy}) is

$$\frac{N_w}{N} = \frac{1}{1 + \frac{1}{4} \left(\frac{L\lambda}{2} \right)^2} \quad (21)$$

where L is the length of cell in the specified direction

We can now calculate the expected σ for different aspect ratios as a function of λ if we take the value of σ in

the ballistic limit and scale it by N_w/N giving

$$\sigma(\lambda) = \sigma_0 \frac{N_w}{N} \quad (22)$$

Where σ_0 is the ballistic limit value of σ . Similarly, the expected $L_{mod}(\lambda)$ would be

$$L_{mod}(\lambda) = (L_{mod0} - L) \frac{N_w}{N} + L = \Delta L_0 \frac{N_w}{N} + L \quad (23)$$

where L_{mod0} is the ballistic limit value of L_{mod} , and $\Delta L_0 = L_{mod0} - L$.

However, when extending this model of the λ dependence to work with σ_v , we need to remember that the width of the v Gaussian comes from asymmetry in the mixing of the x and y components of the velocity, so that the Gaussian gets narrower not simply as wall collisions are reduced but with an additional factor of the relative number of gas collisions between the calculation of S_{yy} (a square with sides L_y) and S_{xx} (a square with sides L_x) for a given λ giving

$$\sigma_v(\lambda) = \sigma_{v0} \frac{1}{1 + \frac{1}{4}a^2 \left(\frac{aL_x\lambda}{2}\right)^2} \quad (24)$$

Where $a = \frac{L_y}{L_x}$, and σ_{v0} is the ballistic limit value of σ_v .

MODEL OF ASPECT RATIO DEPENDENCE IN THE BALLISTIC LIMIT

Although the previous model provides a way to find the spectrum of the correlation function as a function of λ given the ballistic limit correlation function; σ_0 , L_{mod0} , and σ_{v0} still need to be determined for each value of the aspect ratio (a). By understanding how σ_0 , L_{mod0} , and σ_{v0} scale with the aspect ratio of the physical cell it is possible to write the spectrum of the correlation function in a way that depends only on three parameters (σ_{square} , $L_{modsquare}$, and $\sigma_{v,a=\infty}$).

L_{mod0} scaling in terms of the square cell

For a square cell, scaling the cell to a larger square should preserve the change in $L_x \Delta L_x$ as a fraction of L_x in order to keep the same relative change in image positions from the specular case. In the case of a rectangular cell where $L_y > L_x$, with aspect ratio integer $a = \frac{L_y}{L_x}$, we would need a $L_x \times L_x$ square cells along the y direction, as shown in Fig. 3, to make our rectangle. Therefore we might expect to see $\Delta L_y/L_y = a\Delta L_x/L_x$ for this more general case. Assuming this is true we then have

$$\begin{aligned} L_{mody0} &= \frac{\Delta L_{y0}}{L_y} L_y + L_y = a \frac{\Delta L_{x0}}{L_x} L_y + L_y \\ &= a^2 \Delta L_{x0} + a L_x \end{aligned} \quad (25)$$

for a rectangular cell in the ballistic limit, where $\Delta L_{x0} = L_{modsquare} - L$, and $L_{modsquare}$ is the average image cell wall length for a square cell with sides L_x in the ballistic limit.

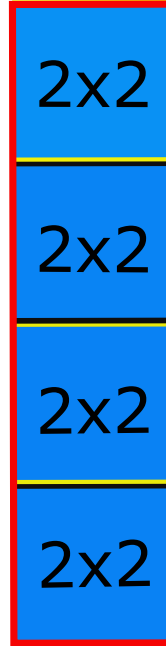


FIG. 3. Diagram of a single 2x8 periodic cell constructed from 4 2x2 image cells. The “real” boundary of the cell is red. The boundary of each 2x2 cell alternates between black or yellow to show the overlap of the boundary between neighboring cells. Note that 6 of the 4 2x2 squares’ walls used to make the rectangular cell are internal to the rectangular cell.

From this same idea we would then also have that $\Delta L_x/L_x$ is independent of the aspect ratio. Also note that in these arguments a is always a positive integer as we are constructing the rectangular cell in units of the $L_x \times L_x$ cell.

σ_{y0} scaling in terms of the square cell

For Lambert scattering walls each wall collision mixes the x and y components of a trajectory. Therefore wall collisions along the x (or y) axis also contribute to σ_y (or σ_x). So in determining σ_{y0} , we start by considering square space $L_y \times L_y$ in size made from $L_x \times L_x$ image cells in an attempt to include the collisions along the x axis that contribute to σ_{y0} . Doing so we would then have

$$\sigma_{y0} = a^2 \sigma_{square} \quad (26)$$

Where σ_{square} is the standard deviation of the image cell wall length for the 2x2 square cell in the ballistic limit. However, this expression fails to take into account

the fact that scaling the standard deviation as if we had $a^2 L_x \times L_x$ square cells results in effectively over estimating the contribution of wall collisions in the y direction. This scaling adds $2(a - 1)$ unphysical internal walls to each physical rectangular cell in the space. See Fig. 3. If we assume every wall of a $L_x \times L_x$ cell equally contributes $1/4\sigma_{square}$ to σ_{y0} , then since there are a rectangular physical cells over the $L_y \times L_y$ space, we find we have overestimated σ_y by $1/2a(a - 1)\sigma_{square}$. Therefore the correct σ_y is

$$\begin{aligned}\sigma_{y0} &= a^2\sigma_{square} - \frac{1}{2}(a^2 - a)\sigma_{square} \\ &= \frac{\sigma_{square}}{2}(a^2 + a)\end{aligned}\quad (27)$$

σ_{x0} scaling in terms of the square cell

Similarly, simply taking $\sigma_{x0} = \sigma_{square}$, will also overestimate the contribution to σ_{x0} made by wall collisions in the y direction. For σ_{y0} we saw the over estimation was $\frac{1}{2}(a^2 - a)\sigma_{square}$ over a $L_y \times L_y$ square space. If we rescale this result for a $L_x \times L_x$ space, we find the overestimate is $\frac{1}{2}\frac{(a^2 - a)}{a^2}\sigma_{square}$. σ_{x0} is then given by

$$\begin{aligned}\sigma_{x0} &= \sigma_{square} \left(1 - \frac{\frac{1}{2}(a^2 - a)}{a^2}\right) \\ &= \frac{\sigma_{square}}{2} \frac{(a^2 + a)}{a^2}\end{aligned}\quad (28)$$

σ_{v0} scaling as a measure of the asymmetry of the cell

As discussed earlier σ_{v0} comes from the asymmetry of the cell. In the case where $L_y \gg L_x$ the situation is effectively 1D and only the y component of the velocity contributes to transport of particles across the cell, but with a spread in the effective velocity in the y direction of the particles determined by the number of collisions in the x direction. Conversely, in the square cell x and y must be weighted equally so the effective velocity in the y direction is always its nominal value of 1. Given the value at $a = \infty$, σ_{v0} could therefore reasonably be scaled by a measure of the asymmetry of the cell giving

$$\begin{aligned}\sigma_{v0}(a) &= \sigma_{v,a=\infty} \frac{A_{yy} - A_{xy}}{A_{yy}} = \sigma_{v,a=\infty} \frac{a^2 L_x^2 - a L_x^2}{a^2 L_x^2} \\ &= \sigma_{v,a=\infty} \frac{a^2 - a}{a^2}\end{aligned}\quad (29)$$

where A_{yy} is the area of a $L_y \times L_y$ square and A_{xy} is the area of a $L_x \times L_y$ rectangle.

COMPARISON TO SIMULATION

Now that we have a model of the λ and aspect ratio dependence, we combine the Eqs. (22)-(24) with Eqs. (25), (27)-(29) to get

$$\sigma_y = \sigma_{square} \frac{a^2 + a}{2 \left(1 + \frac{1}{4} \left(\frac{a L_x \lambda}{2}\right)^2\right)}\quad (30)$$

$$\sigma_x = \sigma_{square} \frac{a^2 + a}{2a^2 \left(1 + \frac{1}{4} \left(\frac{L_x \lambda}{2}\right)^2\right)}\quad (31)$$

$$L_{mody} = a^2 \frac{L_{modsquare} - L_x}{1 + \frac{1}{4} \left(\frac{a L_x \lambda}{2}\right)^2} + a L_x\quad (32)$$

$$L_{modx} = \frac{L_{modsquare} - L_x}{1 + \frac{1}{4} \left(\frac{L_x \lambda}{2}\right)^2} + L_x\quad (33)$$

$$\sigma_v = \sigma_{v,a=\infty} \frac{a^2 - a}{a^2} \frac{1}{1 + \frac{1}{4} a^2 \left(\frac{a L_x \lambda}{2}\right)^2}\quad (34)$$

Leaving us with 3 free parameters σ_{square} , $L_{modsquare}$, and $\sigma_{v,a=\infty}$. These parameters are determined by fitting to simulation.

The simulation calculates trajectories for a uniform distribution of particles in the cell. Over each timestep trajectories have constant velocity, with checks for gas collisions at the end of each timestep. Gas collisions rotate the trajectory to a uniformly distributed random angle, but do not change the magnitude of the velocity. The rate of gas collisions is determined by an exponential distribution with characteristic timescale t_c . The walls of the 2D rectangular cell are Lambert scattering with the scattering angle at each wall collision calculated by $\theta = 2 \arcsin(\sqrt{Rand()}) - \pi/2$, where θ is the scattering angle relative to the normal of the wall and ranges from $-\pi/2$ to $\pi/2$, and $Rand()$ is a function that returns a uniformly distributed random number between 0 and 1, thereby giving a cosine distributed θ . Wall collision times are determined by checking if between the i and the $i+1$ timestep the trajectory will intersect with the wall, and if so calculating a wall collision at the i^{th} time. Small timesteps relative to the ballistic time are needed to accurately calculate the trajectories in the ballistic limit. The simulated trajectories are used to calculate the position-position correlation function. The spectrum is then determined by taking the fast Fourier transform. The simulation only considers $\tau > 0$, where the full spectrum includes negative tau, therefore the real part of the simulation is equal to 1/2 of S_{rr} . Like in our model, times are measured in units of t_b and the speed of the

particles is fixed to 1. Additionally the center of the cell is located at the origin with walls at $\pm L/2$.

Fitting our model to a 4000 particle simulation over 20000 $0.0125t_b$ timesteps of a 2×2 square cell in the ballistic limit ($\lambda = 0.02$) with Lambert scattering walls as shown in Fig. 4 we determine $\sigma_{square} = 0.393$ and $L_{modsquare} = 2.13$. When fitting our model we only use the $n = \pm 1$ terms, assuming the contribution from $|n| > 1$ terms is negligible. To find the value of $\sigma_{v,a=\infty}$ that best fits the simulation, our model (using $\sigma_{square} = 0.393$ and $L_{modsquare} = 2.13$) is fit to a 16000 particle 20000 timestep ballistic limit simulation for a 2×8 rectangular cell ($a = 4$) as shown in Fig. 5. From this fit we find $\sigma_{v,a=\infty} = 0.54$. In all plots comparing the model and simulation only $1/2$ of the S_{rr} calculated from the model is plotted, and only $n = \pm 1$ terms of the calculation are used.

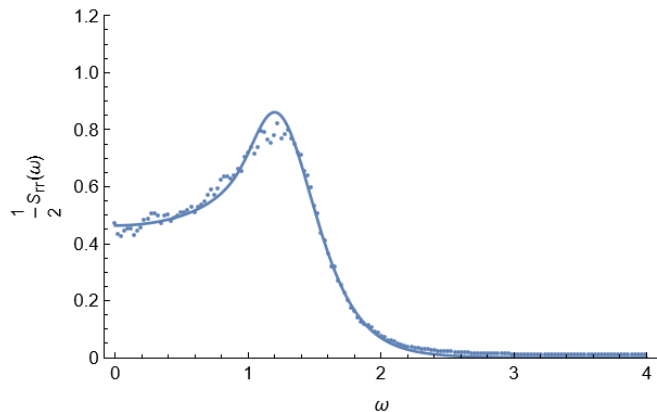


FIG. 4. Simulation of the spectrum of the position-position auto-correlation function for a 2×2 square with Lambert scattering walls in the ballistic limit ($\lambda = 0.02$) along with a fit to the data using the model described by Eq. (19) and Eqs. (30)-(34). From this we find the best fit values for σ_{square} and $L_{modsquare}$ are 0.393 and 2.13 respectively.

Using this model and the parameter values found from fitting the $a = 1$ and $a = 4$ cells, we find good agreement in the ballistic limit for the entire range of aspect ratios from $a = 1$ to $a = 6$ as shown in Fig. 6.

Similarly we see good agreement going from the ballistic to diffusive limit for all aspect ratios, especially for the case of the square cell, with the largest disagreement between model and simulation occurring around the S_{xx} peak at higher aspect ratios. Fig. 7 shows comparisons of our model to simulation from the ballistic to diffusive limit for $a = 1$ through 4. Including the $|n| > 1$ terms in the initial fitting may result in slightly different values of the fitted parameters. For rectangular cells where the spectrum is dominated by S_{yy} this change should be most noticeable in $\sigma_{v,a=\infty}$. Additionally since we only consider $|n| = 1$ the possibility of the fitted parameters having n dependence is not explored.

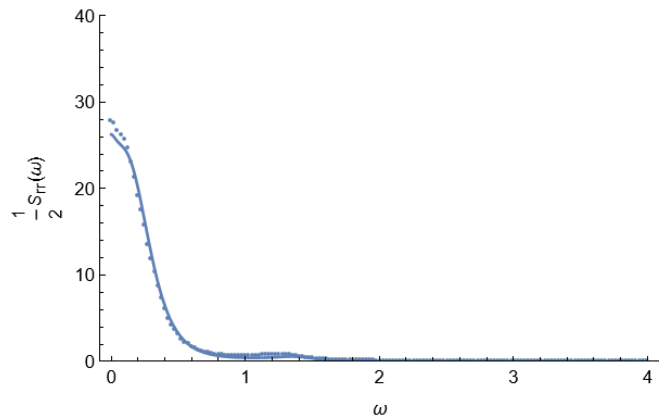


FIG. 5. Simulation of the spectrum of the position-position auto-correlation function for a 2×8 rectangle with Lambert scattering walls in the ballistic limit ($\lambda = 0.02$) along with a fit to the data using the model described by Eq. (19) and Eqs. (30)-(34). From this we find the best fit value for $\sigma_{v,a=\infty} = 0.54$, given $\sigma_{square} = 0.393$ and $L_{modsquare} = 2.13$.

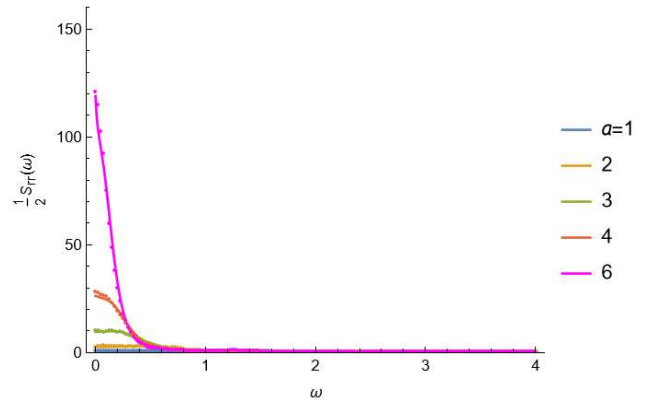


FIG. 6. Simulations of the spectrum of the position-position auto-correlation function between $a = 1$ and $a = 6$ in the ballistic limit ($\lambda = 0.02$) along with the model described in by Eq. (19) and Eqs. (30)-(34) for the same aspect ratios. Model curves are plotted using $\sigma_{v,a=\infty} = 0.54$, $\sigma_{square} = 0.393$, and $L_{modsquare} = 2.13$.

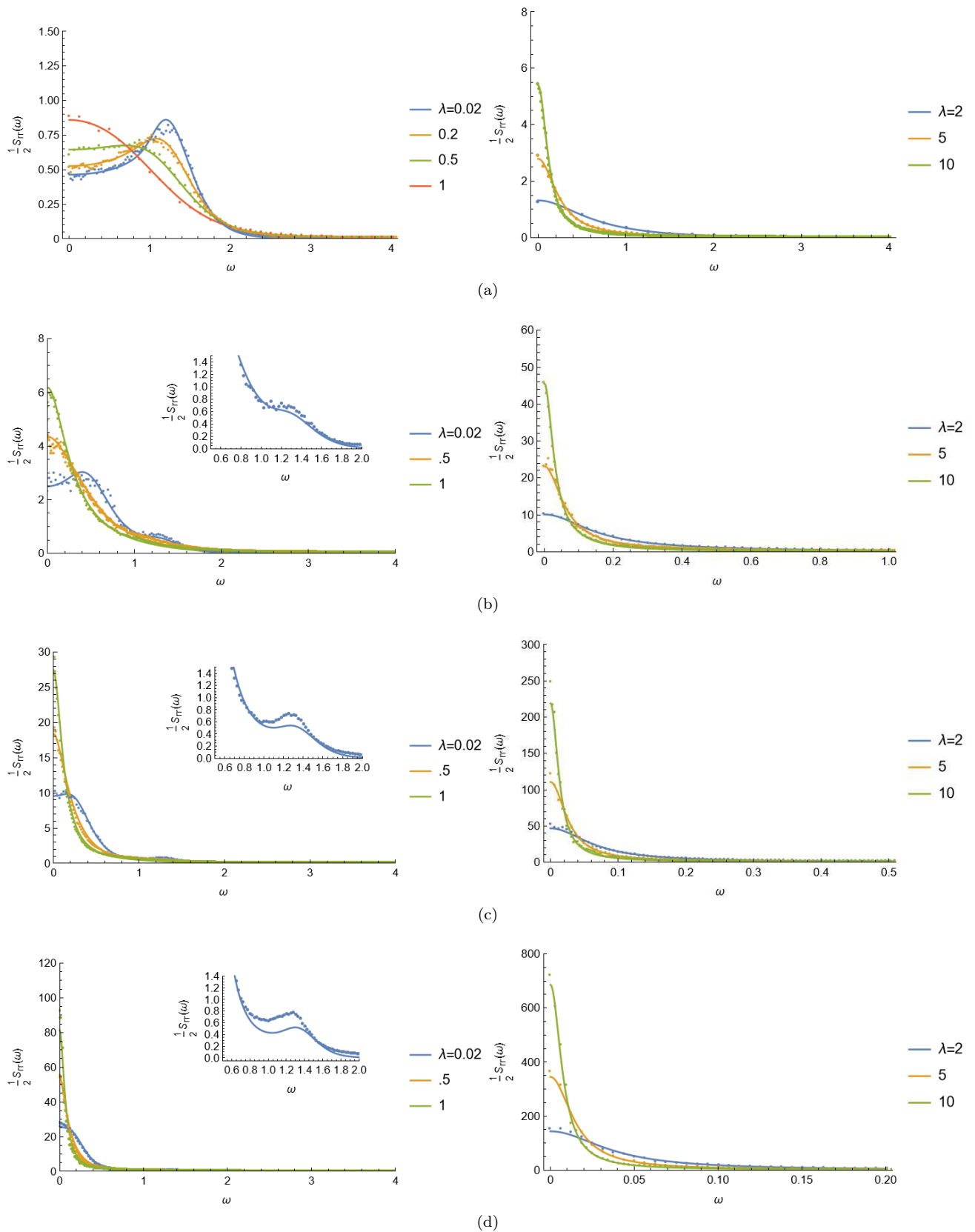


FIG. 7. Simulations of the spectrum of the position-position auto-correlation function from the ballistic to diffusive regime along with the model described in by Eq. (19) and Eqs. (30)-(34). Model curves are plotted using $\sigma_{v,a=\infty} = 0.54$, $\sigma_{square} = 0.393$, and $L_{modsquare} = 2.13$. Curves for aspect ratios of 1, 2, 3, and 4 are plotted in subfigures (a), (b), (c), and (d) respectively, with $\lambda \leq 1$ on the left and $\lambda > 1$ on the right. For the $\lambda \leq 1$ curves of subfigures (b),(c), and (d) we additionally plot a zoomed in view of of the $\lambda = 0.02$ curve to show the peak resulting from S_{xx} contribution to the correlation function. This peak is suppressed at larger λ .

CONCLUSION

In this work we have expanded on the results of [15, 16] and shown how the method of images can be used to model Lambert scattering walls for rectangular cells with reasonable accuracy from the ballistic to diffusive regime for aspect ratios between 1 and 6. This is done by replacing the periodic extension in the method of images used in [15, 16] by a Gaussian distribution of extensions characterized by a standard deviation given by σ_{square} and an average L_{mod} . For rectangular cells a Gaussian spread in the speed is also needed in the S_{yy} spectrum characterized by standard deviation σ_v in order to account for the effects of an asymmetric cell on the x and y components of the velocity after a wall collision. It also should be noted that the Gaussian distributions used in this model are only approximations. The true distributions shouldn't allow negative values of l or v . The resulting correlation function is given by Eq. (19) and Eqs. (30)-(34). Comparing to simulation we find $\sigma_{square} = 0.393$, $L_{modx} = 2.13$, and $\sigma_{v,a=\infty} = 0.54$. With only three free parameters, two of which describe the wall scattering in a

square cell, and a third that describes asymmetry in the mixing of x and y components of the velocity due to wall collisions, this model allows us to describe a remarkably wide range of aspect ratios and gas collision rates, and reproduces the feature of two peaks in the ballistic limit spectrum seen in simulations of rectangular cells. The larger peak coming from the S_{yy} contribution to the spectrum, and the much smaller peak between $\omega = 1.2$ and 1.4 coming from S_{xx} . Although further work is needed to understand the differences between model and simulation in the S_{xx} peak shape. Given that this model works by finding the distribution of triangle periodic extensions that reproduces Lambert scattering, it may be possible to reproduce other wall scattering conditions by finding the appropriate values of σ_{square} , L_{modx} , and $\sigma_{v,a=\infty}$. As such this work has applications for transport in mesoscopic systems with a variety of boundary conditions ranging from purely specular to the purely Lambert scattering case discussed in this work. Additionally the trajectory correlation functions in this work have applications to the problem of spin relaxation and frequency shifts for polarized gasses in inhomogeneous magnetic fields. As well as calculations of the motional field "false nEDM" frequency shift seen in nEDM experiments.

-
- [1] N. Bloembergen, E. Purcell, and R. Pound, Relaxation effects in nuclear magnetic resonance absorption, *Phys. Rev.* 73, 679 (1948)
 - [2] R. Golub, R. M. Rohm, and C. M. Swank, Reexamination of relaxation of spins due to a magnetic field gradient: Identity of the Redfield and Torrey theories, *Phys. Rev. A* 83, 023402 (2011)
 - [3] G. Pignol, M. Guigue, A. Petukhov, and R. Golub, Frequency shifts and relaxation rates for spin-1/2 particles moving in electromagnetic fields, *Phys. Rev. A* 92, 053407 (2015)
 - [4] J. M. Pendlebury, W. Heil, Y. Sobolev, P. G. Harris, J. D. Richardson, R. J. Baskin, D. D. Doyle, P. Geltenbort, K. Green, M. G. D. van der Grinten, P. S. Iaydjiev, S. N. Ivanov, D. J. R. May, and K. F. Smith, Geometric-phase-induced false electric dipole moment signals for particles in traps, *Phys. Rev. A* 70, 032102 (2004)
 - [5] A. Redfield, On the theory of relaxation processes, *IBM J. Res. Dev.* 1, 19 (1957)
 - [6] C. P. Slichter, *Principles of Magnetic Resonance*, 3rd ed. (Springer, Berlin-Heidelberg, 1996)
 - [7] D. D. McGregor, Transverse relaxation of spin-polarized ^3He gas due to a magnetic field gradient, *Phys. Rev. A* 41, 2631 (1990)
 - [8] S. K. Lamoreaux and R. Golub, Detailed discussion of a linear electric field frequency shift induced in confined gases by a magnetic field gradient: Implications for neutron electric-dipole-moment experiments, *Phys. Rev. A* 71, 032104 (2005)
 - [9] A. K. Petukhov, G. Pignol, D. Jullien, and K. H. Andersen, Polarized ^3He as a Probe for Short-Range Spin-Dependent Interactions, *Phys. Rev. Lett.* 105, 170401 (2010)
 - [10] S. M. Clayton, Spin relaxation and linear-in-electric-field frequency shift in an arbitrary, time-independent magnetic field, *J. Magn. Reson.* 211, 89 (2011)
 - [11] A. L. Barabanov, R. Golub, and S. K. Lamoreaux, Electric dipole moment searches: Effect of linear electric field frequency shifts induced in confined gases, *Phys. Rev. A* 74, 052115 (2006)
 - [12] R. Golub, A. Steyerl, C. Kaufman, and G. Müller, Geometric phases in electric dipole searches with trapped spin-1/2 particles in general fields and measurement cells of arbitrary shape with smooth or rough walls, *Phys. Rev. A* 92, 06123 (2015)
 - [13] A. Steyerl, C. Kaufman, G. Müller, S. S. Malik, A. M. Desai, and R. Golub *Phys. Rev. A* 89, 052129 (2014)
 - [14] S. M. Clayton, Spin relaxation and linear-in-electric-field frequency shift in an arbitrary, time-independent magnetic field, *J. Magn. Reson.* 211, 89 (2011)
 - [15] C. M. Swank, A. K. Petukhov, and R. Golub, Correlation functions for restricted Brownian motion from the ballistic through to the diffusive regimes, *Phys. Lett. A* 376, 2319 (2012)
 - [16] C. M. Swank, A. K. Petukhov, and R. Golub, Random walks with thermalizing collisions in bounded regions: Physical applications valid from the ballistic to diffusive regimes *Phys. Rev. A* 93, 062703 (2016)
 - [17] J. Masoliver, J. M. Porra, and G. H. Weiss, Some two- and threedimensional persistent random walks, *Phys. A (Amsterdam, Neth.)* 193, 469 (1993)